*J. Fluid Mech.* (2001), *vol.* 434, *pp.* 355–369. Printed in the United Kingdom



# Transitions and instabilities of flow in a symmetric channel with a suddenly expanded and contracted part

By J. MIZUSHIMA AND Y. SHIOTANI

Department of Mechanical Engineering, Doshisha University, Kyotanabe, Kyoto 610-0321, Japan

(Received 7 March 2000 and in revised form 3 November 2000)

Transitions and instabilities of two-dimensional flow in a symmetric channel with a suddenly expanded and contracted part are investigated numerically by three different methods, i.e. the time marching method for dynamical equations, the SOR iterative method and the finite-element method for steady-state equations. Linear and weakly nonlinear stability theories are applied to the flow. The transitions are confirmed experimentally by flow visualizations. It is known that the flow is steady and symmetric at low Reynolds numbers, becomes asymmetric at a critical Reynolds number, regains the symmetry at another critical Reynolds number and becomes oscillatory at very large Reynolds numbers. Multiple stable steady-state solutions are found in some cases, which lead to a hysteresis. The critical conditions for the existence of the multiple stable steady-state solutions are determined numerically and compared with the results of the linear and weakly nonlinear stability analyses. An exchange of modes for oscillatory instabilities is found to occur in the flow as the aspect ratio, the ratio of the length of the expanded part to its width, is varied, and its relation with the impinging free-shear-layer instability (IFLSI) is discussed.

## 1. Introduction

Flow in a two-dimensional symmetric channel with a suddenly expanded and contracted part is one of the simplest models that is not homogeneous in the flow direction. Theoretical analyses were difficult for such a flow because of the inhomogeneity. In particular, traditional stability theories for parallel flows could not be easily applied to the flow. So, instabilities and transitions of the flow have been investigated mainly by numerical methods and shown to include rich phenomena.

Transitions of flow in a symmetric channel with a sudden expansion have been investigated extensively. This is a special case of the symmetric channel with a suddenly expanded and contracted part. For instance, Durst, Melling & Whitelaw (1974) and Cherdron, Durst & Whitelaw (1978) measured velocity profiles in detail for the symmetric sudden expansion flow by laser-Doppler velocimetry (LDV) and flow-visualization methods. It was found that the flow is symmetric at low Reynolds numbers, but becomes asymmetric at higher Reynolds numbers. Oscillatory flows are also observed at very high Reynolds numbers.

It was shown by Fearn, Mullin & Cliffe (1990) that the asymmetry arises at a critical Reynolds number owing to a pitchfork bifurcation. They measured the degree of asymmetry experimentally and compared it with their numerical results. The coincidence of the experimental and numerical results was satisfactory except in the

immediate vicinity of the bifurcation. They modelled the effect of small imperfections in the flow channel numerically and clarified that the disconnection observed in the experimental bifurcation diagram is due to small imperfections that are inevitably present in the experimental apparatus.

Linear stability of the flow in the channel was studied by Alleborn *et al.* (1997), who also made a systematic bifurcation analysis and obtained a bifurcation diagram of the steady-state solutions including up to the third bifurcation points of the symmetric flow.

Weakly nonlinear stability theory was successfully applied to the flow in the channel by Mizushima & Shiotani (2000). They considered a slight asymmetric channel as an imperfection of the system and derived an amplitude equation for a disturbance by including the effect of the imperfection. The equilibrium amplitude of the disturbance evaluated by the amplitude equation was shown to be in good agreement with the experimental results by Fearn *et al.* (1990) for the flow in a symmetric channel that is presumed symmetric.

Flows in a two-dimensional symmetric channel with a suddenly expanded and contracted part were investigated by Mizushima, Okamoto & Yamaguchi (1996 hereinafter referred to as MOY). They made numerical simulations for the flow and analysed the numerical data by applying the bifurcation theory. It was found that the flow is steady and symmetric at low Reynolds numbers, becomes asymmetric at a critical Reynolds number $Re_{c1}$ owing to a symmetry-breaking pitchfork bifurcation and regains the symmetry at $Re_{c2}(>Re_{c1})$ owing to another pitchfork bifurcation. The symmetric flow was shown to become oscillatory at $Re_{c3}$ owing to a Hopf bifurcation. They evaluated the critical values of $Re_{c1}$, $Re_{c2}$ and $Re_{c3}$, and obtained a transition diagram of the flow. However, the bifurcation diagrams obtained were incomplete because they included unexpected discontinuous lines in place of the smooth continuous lines presumed.

In the present paper, we investigate transitions and instabilities of the flow in a symmetric channel with a suddenly expanded and contracted part experimentally, numerically and theoretically. We measure the velocity by LDV and examine the flow patterns by flow visualizations in experiments, and use three different methods in numerical calculations, i.e. the time marching method for dynamical equations, the SOR iterative method and the finite-element method for steady-state equations. The weakly nonlinear stability theory is applied to the flow to elucidate the bifurcation structure near the critical Reynolds numbers for the pitchfork bifurcations. This work is an extension of MOY. We focus our attention on multiple stable steady-state solutions of the flow at relatively low Reynolds numbers, which lead to a hysteresis. Our attention is also focused on the impinging free-shear-layer instability, which makes the flow oscillatory. The impinging free-shear-layer instability is characterized by a stepwise change of the Strouhal number with a continuous change of parameter and observed when a jet-like stream impinges on an object with a corner edge (Rockwell & Naudascher 1979).

## 2. Problem description

We consider a symmetric channel with a suddenly expanded and contracted part as shown in figure 1. Flow comes in from the inlet AB of width $h$, enters the suddenly expanded part DEJK through the sudden expansion LC, leaves it through the sudden contraction IF and goes out from the outlet HG of width $h$. The expansion ratio $E$ is defined as $E = \mathrm{EF}/\mathrm{AB}$ and is fixed as $E = 3$ in the present study. This case has

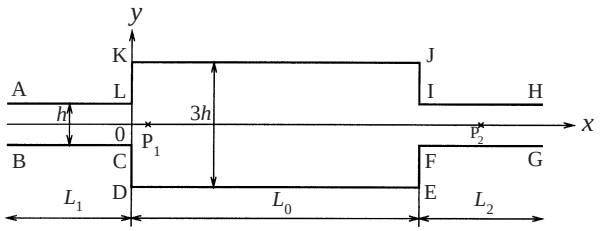


FIGURE 1. Coordinates and geometry.

been investigated most extensively. The aspect ratio $A$ is defined as

$$A = L_0/3h = \mathrm{DE/KD} \tag{2.1}$$

where $L_0$ is the length of the suddenly expanded part.

The mathematical formulation for the present problem is given in Mizushima & Shiotani (2000), so we summarize it briefly. We assume an incompressible and two-dimensional flow field. The governing equations for the velocity $\boldsymbol{u} = (u, v)$ and the pressure $p$ are the Navier–Stokes equation and the continuity equation. As the flow is assumed to be two-dimensional, the stream function can be introduced. We adopt the stream function $\psi(x, y, t)$ and the vorticity $\omega(x, y, t)$ formulation except for numerical calculations of unstable steady-state solutions by the finite-element method where primitive variables $\boldsymbol{u}$ and $p$ are used. The basic equations are the vorticity transport and the Poisson equations for $\omega$ and $\psi$, which are written as

$$M\frac{\partial \psi}{\partial t} = L\psi + ReN(\psi, \psi), \tag{2.2}$$

where $M \equiv \Delta$, $L \equiv \Delta\Delta$, $N(f, g) \equiv J(f, \Delta g)$ and

$$\Delta \equiv \frac{\partial^2}{\partial x^2} + \frac{\partial^2}{\partial y^2}, \quad J(f, g) \equiv \frac{\partial f}{\partial x}\frac{\partial g}{\partial y} - \frac{\partial f}{\partial y}\frac{\partial g}{\partial x}.$$

All the variables are normalized by using the maximum inlet velocity $U_{\max}$ and the half width $\frac{1}{2}h$ of the inlet channel as representative velocity and lengthscales. The time $t$ is normalized by $v/U_{\max}^2$ and the Reynolds number is defined as

$$Re = U_{\max}h/2v.$$

The boundary condition at AB (figure 1) is assumed as a fully developed plane Poiseuille flow. The outlet condition at HG is

$$\frac{\partial^2 \psi}{\partial x^2} = 0, \quad \frac{\partial^2 \omega}{\partial x^2} = 0, \tag{2.3}$$

when the flow is steady. The Sommerfeld radiation condition is adopted for time-periodic flows by using the convection equation at the outlet as

$$\frac{\partial \psi}{\partial t} + c\frac{\partial \psi}{\partial x} = 0, \quad \frac{\partial \omega}{\partial t} + c\frac{\partial \omega}{\partial x} = 0, \tag{2.4}$$

where $c$ is a phase velocity of outgoing waves. For the value of $c$, the outlet velocity of $u$ at each position on HG is used in the present study. The boundary conditions on all the walls are the non-slip condition.

Steady-state solutions $\overline{\psi}(x, y)$ and $\overline{\omega}(x, y)$ satisfy the steady-state vorticity transport equation and the Poisson equation, which are obtained by dropping the time derivative

term in (2.2) as

$$L\overline{\psi} + ReN(\overline{\psi}, \overline{\psi}) = 0. \tag{2.5}$$

It is known that there exist steady symmetric solutions for all values of $Re$. We adopt the symmetric solution as the basic flow for the linear and weakly nonlinear stability analyses.

Linear stability of the symmetric steady flow ($\overline{\psi}$, $\overline{\omega}$) is investigated by adding a disturbance ($\psi'$, $\omega'$) to it. The linear stability equation is expressed as

$$\lambda M\widehat{\psi} = L\widehat{\psi} + ReN(\overline{\psi}, \widehat{\psi}) + ReN(\widehat{\psi}, \overline{\psi}), \tag{2.6}$$

where the time dependence of the disturbance is assumed as $\psi' = \widehat{\psi}(x, y)\exp(\lambda t)$ and $\omega' = \widehat{\omega}(x, y)\exp(\lambda t)$. The boundary conditions for ($\widehat{\psi}$, $\widehat{\omega}$) at the inlet and the outlet are

$$\widehat{\psi} = 0, \quad \frac{\partial\widehat{\psi}}{\partial x} = 0, \quad \frac{\partial\widehat{\omega}}{\partial x} = 0 \quad \text{on AB},$$

$$\frac{\partial^2\widehat{\psi}}{\partial x^2} = 0, \quad \frac{\partial^2\widehat{\omega}}{\partial x^2} = 0 \quad \text{on HG}.$$

The non-slip condition is adopted on all the wall boundaries. The complex linear growth rate $\lambda$ is found by solving equation (2.6) under the boundary conditions with the SOR iterative method. The real part of $\lambda$, say $\lambda_r$, indicates the linear growth rate of the disturbance. The Reynolds number $Re$ at which $\lambda_r$=0 gives the critical Reynolds number $Re_c$. If the imaginary part of $\lambda$, say $\lambda_i$, is zero, the principle of the exchange of stabilities is valid. Then, the eigenfunctions ($\widehat{\psi}$, $\widehat{\omega}$) at the critical state are real. It is known that the eigenfunction $\widehat{\psi}$ for the most unstable mode is symmetric along the $x$-axis.

We consider the weakly nonlinear behaviour of the disturbance added to the symmetric flow near the critical states of the pitchfork bifurcations. It is known that there are two pitchfork bifurcation points for the flow in a symmetric channel with a suddenly expanded and contracted part, where the symmetric flow becomes asymmetric at $Re = Re_{c1}$ and the asymmetric flow recovers its symmetry at $Re = Re_{c2}$. For the local bifurcation analysis near the critical state at $Re \gtrsim Re_{c1}$, we adopt $\epsilon$, defined by $\epsilon^2 \equiv Re - Re_{c1}$ as a small parameter, where we denote $Re_{c1}$ by $Re_c$ hereinafter. We expand physical quantities such as $\overline{\psi}$, $\psi'$ and $t$ in $\epsilon$ as

$$\psi' = \epsilon\widetilde{\psi}_1 + \epsilon^2\widetilde{\psi}_2 + \epsilon^3\widetilde{\psi}_3 + \cdots,$$

$$\overline{\psi} = \overline{\psi}_0 + \epsilon^2\overline{\psi}_1 + \cdots,$$

$$\frac{\partial}{\partial t} = \frac{\partial}{\partial t_0} + \epsilon^2\frac{\partial}{\partial t_1} + \cdots. \tag{2.7}$$

It is noted that the steady flow is also expanded in $\epsilon$ and that $\overline{\psi}_0 = \overline{\psi}(Re_c)$ and $\overline{\psi}_1 = (\partial\psi/\partial Re)_{Re=Re_c}$.

The amplitude equation is obtained from the solvability condition for the third-order equation of $O(\epsilon^3)$ as

$$\frac{\mathrm{d}v_1}{\mathrm{d}t} = \lambda_1(Re - Re_c)v_1 + \lambda_2{v_1}^3, \tag{2.8}$$

where $v_1$ is the velocity component in the $y$-direction at a representative point $P_1 = (x_1, y_1) = (0.8, 0)$ (figure 1). The equilibrium amplitude $v_1$ for the pitchfork

bifurcation is evaluated from (2.8) as

$$v_1 = \pm\sqrt{-\frac{\lambda_1(Re - Re_c)}{\lambda_2}}, \tag{2.9}$$

if $\lambda_1\lambda_2(Re - Re_c) < 0$.

## 3. Numerical methods

### 3.1. *Time-marching method*

In numerical simulations by the time-marching method, an equally spaced mesh system with $\Delta x = \Delta y = 0.1$ is used. The vorticity transport equation is solved by the explicit Euler method with the first-order accuracy in time together with the second-order accuracy of central finite difference in space. The time increments $\Delta t$ are chosen as $\Delta t = 0.001$ or $\Delta t = 0.0005$. The Poisson equation is discretized by the second-order central finite difference and solved by the SOR method, where the relaxation factor $\epsilon$ is kept as $\epsilon = 1.5$. The convergence of the SOR method is determined when the maximum relative error reaches $10^{-5}$ and the steady-flow state is determined when the stream function becomes time independent and the maximum relative error reaches $10^{-10}$.

### 3.2. *SOR iterative method*

Both the steady-state vorticity transport equation and the Poisson equation are solved by the SOR iterative method to calculate steady-state solutions. Spatial derivatives are approximated by the fourth-order finite differences. The relaxation factor $\epsilon$ for the SOR method is determined by considering aspect ratios and Reynolds numbers in the range $0.7 < \epsilon < 1.0$. The convergence of the SOR method is determined when the maximum relative error reaches $10^{-10}$. In order to calculate unstable steady symmetric solutions above a critical Reynolds number, the SOR method is used under the symmetry condition along the centreline of the channel. This method is used also for the numerical evaluation of the linear growth rate and the numerical calculations in the weakly nonlinear stability analysis.

### 3.3. *Finite-element method*

The finite-element method is used to calculate the unstable steady-state asymmetric solutions. The computational domain is divided by triangular elements in the finite-element method. Primitive variables $(\overline{u}, \overline{v})$ and $\overline{p}$ are used for the numerical calculations. The velocity components $\overline{u}$ and $\overline{v}$ are approximated by quadratic polynomial expressions using six nodes in each element and the pressure $\overline{p}$ is approximated by a linear function expression using three points. These expressions for $\overline{u}$, $\overline{v}$ and $\overline{p}$ are substituted in the steady-state Navier–Stokes equation, and the continuity equation. The boundary conditions for $\overline{u}$, $\overline{v}$ and $\overline{p}$ are assumed to be the fully developed Poiseuille flow at the inlet AB (figure 1), $\overline{p} = 0$ at the outlet HG and the non-slip condition on all the walls. The discretized equations are obtained by using the Galerkin method and are solved numerically by using the Newton–Raphson method. The node number used is 4163 and the element number is 1992 for $A = \frac{8}{3}$. The convergence of the Newton–Raphson method is determined when the maximum relative error reaches $10^{-10}$.

## 4. Experimental method

We examine the flow patterns experimentally by flow visualizations. In experiments, water is supplied to the inlet section AB by a pump from a reservoir tank, enters the suddenly expanded and contracted part, goes out from the outlet section HG and comes back to the reservoir tank. The channel is made of transparent acrylic plates. The width $h$ of the inlet section is 5 mm and the channel depth is $12h$ which may satisfy the assumption of a two-dimensional flow field (see figure 1). Both the lengths of the inlet and outlet sections $L_1$ and $L_2$ are 550 mm. The flow was almost a fully developed plane Poiseuille flow at the end of the inlet section. Our experiment was carried out for two different aspect ratios such as $A = \frac{4}{3}$ and $A = \frac{7}{3}$. Aluminium powder is mixed with water for flow visualizations. The maximum inlet velocity $U_{\max}$ is measured at the centre of the inlet AB by LDV. The velocity is controlled by six valves between the tank and the inlet section and the range of the Reynolds number was $0 - 1500$. A sheet of light is thrown by a projector, and traces of reflected light are taken as streamlines by a camera in flow visualizations.

## 5. Results

### 5.1. *Transitions of the flow*

Transitions of the flow for the case of $A = \frac{7}{3}$ were investigated by MOY, so their results are reviewed briefly in order to compare our experimental results with theirs. The flow is steady and symmetric at low Reynolds number, becomes steady but asymmetric at $Re_{c1} = 47.7$ owing to the pitchfork bifurcation and regains the symmetry at $Re_{c2} = 65.2$ owing to the second pitchfork bifurcation for $A = \frac{7}{3}$. The steady symmetric flow becomes oscillatory at $Re_{c3} = 843$ owing to the Hopf bifurcation.

As typical examples, we show numerical and experimental results for the flow patterns at $Re = 40$, 58, 100 in figure 2(*a–f*), where figures 2(*a*), 2(*c*) and 2(*e*) are the flow fields (stream lines) obtained numerically, and others experimentally. The flow is steady and symmetric at $Re = 40$ (figures 2*a* and 2*b*). It has two recirculation vortices with equal lengths in the suddenly expanded part. At $Re = 58$, the flow is steady but asymmetric, bending to one sidewall in the expanded part (figures 2*c* and 2*d*). The direction of the bend is determined by chance with an equal probability for two directions. The flow becomes symmetric again having two large recirculation vortices which extend in the full length of the expanded part at $Re = 100$ (figures 2*e* and 2*f*). At $Re = 900$, the flow is periodic in time. A snapshot of the flow pattern at $Re = 900$ is depicted in figure 3. Circulation vortices generated at the sudden contraction move up and down periodically (figure 3).

The bifurcation diagrams for $A = \frac{7}{3}$ are reproduced in figures 4 and 5. The solid and dashed lines indicate the stable and unstable solutions, respectively, in these figures. The bifurcation diagram for the pitchfork bifurcations is shown in figure 4. We adopt the velocity $v_1$ in the $y$-direction at $P_1(x, y) = (0.8, 0)$ (figure 1) as a representative value manifesting the magnitude of the asymmetry in figure 4. For Reynolds numbers smaller than $Re_{c1}(= 47.7)$, there is only one stable steady solution with $v_1 = 0$, where the flow is symmetric. At $Re_{c1}$, the line of $v_1$ branches into three, which shows that there appear two stable asymmetric solutions while the symmetric solution becomes unstable. The two stable and one unstable solutions join into one stable solution at $Re_{c2}(= 65.2)$, which shows the second pitchfork bifurcation.

The bifurcation diagram for the Hopf bifurcation is shown in figure 5. We adopt an oscillation amplitude $a$ of the velocity $v_2$ at $P_2(x, y) = (17, 0)$ (figure 1) as a

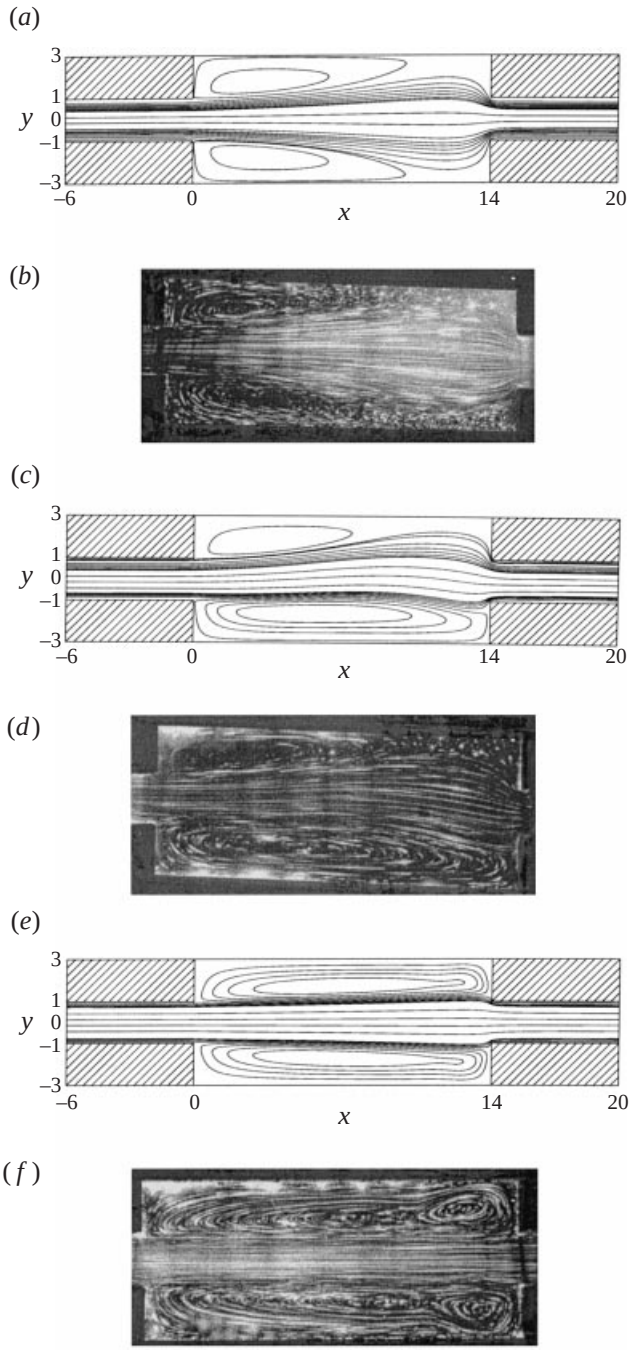


FIGURE 2. Flow patterns. $A = \frac{7}{3}$. (*a*), (*b*) $Re = 40$. (*c*), (*d*) $Re = 58$. (*e*), (*f*) $Re = 100$. (*a*), (*c*), (*e*) Numerical results. (*b*), (*d*), (*f*) Flow visualizations.

representative value manifesting the magnitude of the amplitude of the oscillatory flow in this figure. The steady-state solution is unique for $Re_{c2} < Re < Re_{c3}$ as seen from figure 5, which is a stable symmetric flow. The symmetric flow becomes unstable and an oscillatory flow appears at $Re_{c3} = 843$ owing to the Hopf bifurcation.

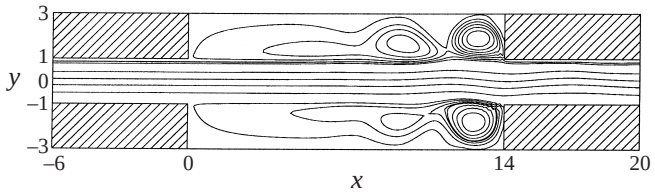


FIGURE 3. A snapshot of the flow pattern. $Re = 900$. $A = \frac{7}{3}$. Numerical results.

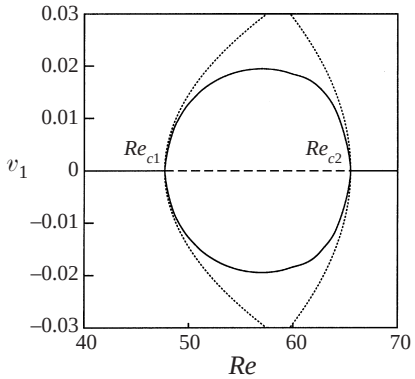


FIGURE 4. Bifurcation diagram. $A = \frac{7}{3}$. The velocity $v_1$ against the Reynolds number $Re$. $v_1$, the velocity $v$ at $P_1(x, y) = (0.8, 0.0)$. —, numerical result; $\cdots$, weakly nonlinear stability theory.

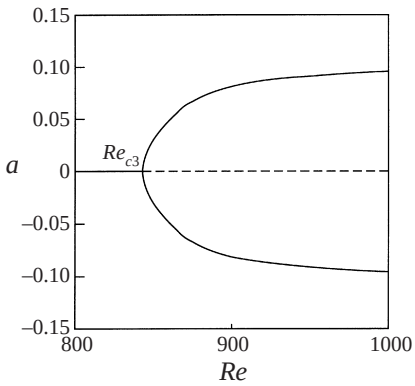


FIGURE 5. Hopf bifurcation diagram. $A = \frac{7}{3}$. The amplitude $a$ against the Reynolds number $Re$. $a$, the oscillation amplitude of the velocity $v$ at $P_2(x, y) = (17.0, 0.0)$.

The bifurcation diagram for $A = \frac{8}{3}$ was shown to be different from that for $A = \frac{7}{3}$ by MOY, but it was incomplete because the solution lines for $v_1$ have discontinuities in the place of the continuous lines presumed. MOY speculated that the jumps occur because of the inverse pitchfork bifurcation. We confirm their speculation by numerical calculations of unstable solutions, which was missing in MOY, by using the finite-element method. We have calculated the steady solutions for $A = \frac{8}{3}$ in detail and obtained a more complete bifurcation diagram as shown in figure 6. The solid and dashed lines indicate the stable and unstable steady-state solutions, respectively. The symmetric unstable solutions AD with $v_1 = 0$ were obtained by the SOR method with the finite-difference approximation under the symmetry condition along the

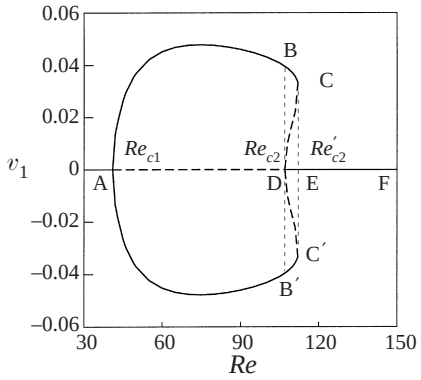


FIGURE 6. Bifurcation diagram. $A = \frac{8}{3}$. $v_1$, the velocity $v$ at $P_1(x, y) = (0.8, 0.0)$.

centreline, whereas the unstable solutions CD and C′D with $v_1 \neq 0$ were obtained by the finite-element method. The first symmetry-breaking pitchfork bifurcation occurs at A in figure 6, where the symmetric solution becomes unstable. The bifurcated solutions are indicated by ABC and AB′C′. The asymmetric solution ABC and AB′C′ are stable, but make saddle node bifurcations at C and C′ ($Re = Re'_{c2}$), respectively. The asymmetric solutions CD and C′D are unstable and the symmetric solution DF is stable. So, there are three stable solutions and two unstable solutions in the range of $Re_{c2} < Re < Re'_{c2}$. The critical values of the pitchfork and saddle node bifurcations are evaluated numerically as $Re_{c1} = 41.0$, $Re'_{c2} = 112$ and $Re_{c2} = 107$, the former two of which are in good agreement with those obtained by MOY, whereas $Re_{c2} = 107$ had not been obtained by them.

We can easily imagine from figure 6 that there occurs a hysteresis. If the Reynolds number is increased from a small value, the symmetric solution bifurcates at A. The bifurcated solution takes a route indicated by ABCEF or AB′C′EF. This shows that the asymmetric flow indicated by ABC (or AB′C′) makes a transition from C to E at $Re = Re'_{c2}$. On the other hand, if the Reynolds number is decreased from a large value, the symmetric flow FED becomes unstable at D, makes a transition to B (or B′) at $Re = Re_{c2}$ and takes a route indicated by BA (or B′A). Thus, the hysteresis occurs in the range of $Re_{c2} \leqslant Re \leqslant Re'_{c2}$.

The flow patterns of the stable symmetric, the stable asymmetric and the unstable asymmetric solutions at $Re = 110$ ($Re_{c2} < 110 < Re'_{c2}$) are shown in figure 7. There are two large recirculation vortices which extend in the full length of the expanded part in the stable symmetric flow (figure 7*a*). The stable asymmetric flow (figure 7*b*) bends much more than the unstable asymmetric flow (figure 7*c*) as seen also from figure 6.

### 5.2. *Linear and weakly nonlinear stabilities*

We have evaluated the linear growth rate of the steady symmetric flow by solving (2.6) under the appropriate boundary condition by the SOR iterative method. In the SOR iterative method, we have assumed the linear growth rate $\lambda$ as well as $\psi$ and $\omega$ as unknown variables, and imposed a normalization condition that the velocity $v_1$ in the $y$-direction at $P_1 = (0.8, 0)$ is unity. The linear growth rate $\lambda$ was obtained as a real value, which means that the principle of the exchange of stabilities is valid in the range of the Reynolds number investigated. The linear growth rate $\lambda$ is depicted for $A = \frac{7}{3}$ in figure 8. Needless to say, the critical Reynolds numbers $Re_{c1}$ and $Re_{c2}$

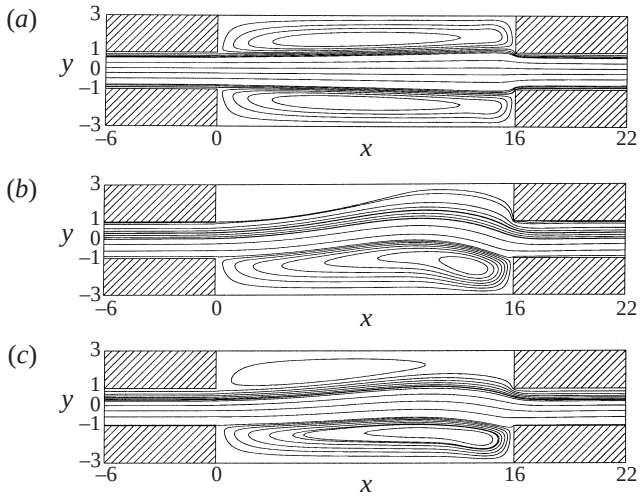


FIGURE 7. Flow patterns. $Re = 110$. $A = \frac{8}{3}$. (*a*) Stable symmetric flow. (*b*) Stable asymmetric flow. (*c*) Unstable asymmetric flow.

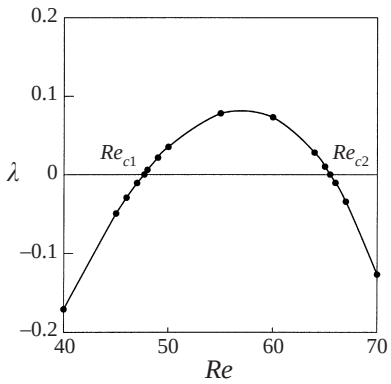


FIGURE 8. Linear growth rate $\lambda$ against the Reynolds number $Re$. $A = \frac{7}{3}$.

agree with the values obtained by the bifurcation analysis of the numerical data. It is seen that the symmetric flow is unstable in the range of $Re_{c1} < Re < Re_{c2}$ and that it is stable out of the range.

The weakly nonlinear stability theory is applied near the pitchfork bifurcation points at $Re_{c1}$ and $Re_{c2}$. We evaluated the coefficients $\lambda_1$ and $\lambda_2$ in the amplitude equation (2.8) numerically to compare the amplitude evaluated from it with the numerical results of the steady-state solution. Values of the coefficients $\lambda_1$ and $\lambda_2$ obtained are shown in table 1, where the critical values $Re_{c1}$ and $Re_{c2}$ are also tabulated for various values of $A$.

We depict the values of $v_1$ evaluated from the equilibrium amplitude (2.9) by dotted lines for $A = \frac{7}{3}$ in figure 4 where the two dotted lines correspond to the bifurcated solutions from $Re_{c1}$ and $Re_{c2}$, respectively. It is seen from figure 4 that there occur supercritical pitchfork bifurcations at the critical Reynolds numbers $Re_{c1}$ and $Re_{c2}$ for $A = \frac{7}{3}$. The weakly nonlinear stability analysis is revealed to play an important role in predicting a parameter region where multiple stable solutions exist although the coincidences of the results of the weakly nonlinear stability analysis and the

| $A$ | $Re_c$ | $\lambda_1$ | $\lambda_2$ |
|---|---|---|---|
| 2.333(= 140/60) | $Re_{c1} = 47.7$ | $1.681 \times 10^{-2}$ | $-1.825 \times 10^{2}$ |
| | $Re_{c2} = 65.5$ | $-2.044 \times 10^{-2}$ | $-1.553 \times 10^{2}$ |
| 2.417(= 145/60) | $Re_{c1} = 44.2$ | $2.593 \times 10^{-2}$ | $-1.777 \times 10^{-2}$ |
| | $Re_{c2} = 76.9$ | $-3.932 \times 10^{-2}$ | $-4.804 \times 10^{1}$ |
| 2.467(= 148/60) | $Re_{c1} = 43.2$ | $2.898 \times 10^{-2}$ | $-1.673 \times 10^{2}$ |
| | $Re_{c2} = 82.9$ | $-4.598 \times 10^{-2}$ | $6.674 \times 10^{1}$ |
| 2.500(= 150/60) | $Re_{c1} = 42.7$ | $3.074 \times 10^{-2}$ | $-1.636 \times 10^{2}$ |
| | $Re_{c2} = 86.8$ | $-5.111 \times 10^{-2}$ | $1.579 \times 10^{2}$ |

TABLE 1. Values of the coefficients $\lambda_1$ and $\lambda_2$ in the amplitude equation.

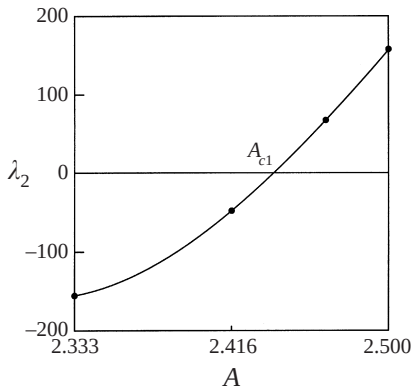


FIGURE 9. Values of the coefficient $\lambda_2$ in the amplitude equation against the aspect ratio $A$.

numerical results of the equilibrium solution are rather limited to the vicinity of the critical Reynolds numbers in figure 4.

We found in the previous subsection that the bifurcation at $Re_{c2}$ is a subcritical pitchfork bifurcation for $A = \frac{8}{3}$. It means that the bifurcation changes from the supercritical to the subcritical one between $A = \frac{7}{3}$ and $\frac{8}{3}$ as $A$ increases. The change of the bifurcation characteristic is indicated by the sign of the coefficient $\lambda_2$ at $Re_{c2}$ in the amplitude equation (2.9). We have evaluated the value of $\lambda_2$ for various values of $A$. The coefficient $\lambda_2$ is plotted against the aspect ratio $A$ in figure 9 where the bifurcation at $Re_{c2}$ is supercritical if $\lambda_2 < 0$ or subcritical if $\lambda_2 > 0$. It is seen that the bifurcation characteristic changes at $A_{c1} = 2.44$.

### 5.3. *Transition diagram*

We made numerical calculations of the steady-state and the time-periodic solutions for various values of $A$ and obtained a transition diagram as summarized in figure 10. For $A < A_{c2} = 2.3$, the flow does not experience any pitchfork bifurcations and makes a transition from a steady symmetric flow to an oscillatory flow at $Re_{c3}$ (line with filled squares in figure 10). For $A > A_{c2}$, the flow undergoes a transition from a steady symmetric flow to a steady asymmetric flow at $Re_{c1}$ (line with filled circles) owing to the symmetry-breaking pitchfork bifurcation, and becomes symmetric again at $Re_{c2}$ (line with open circles). There are multiple stable solutions in the range between $Re_{c2}$ and $Re'_{c2}$ for $A > A_{c1}$ (the region between two lines with open circles and filled circles). So the hysteresis occurs in this range. The steady flow makes a transition

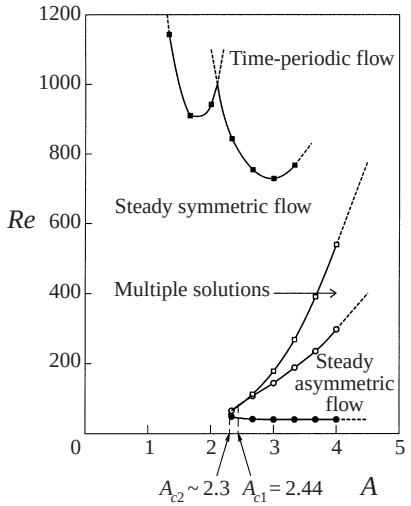


FIGURE 10. Transitions of the flow. ●, the first pitchfork bifurcation points $Re_{c1}$; ○, the second pitchfork bifurcation points $Re_{c2}$; □, saddle node bifurcation points $Re'_{c2}$; ■, Hopf bifurcation points $Re_{c3}$.

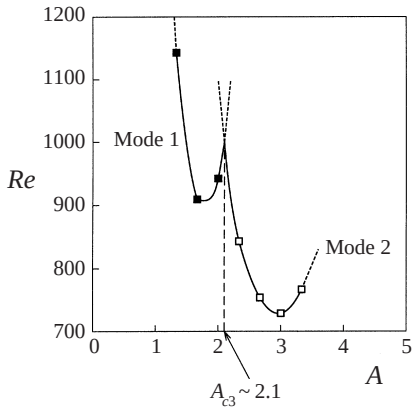


FIGURE 11. Transition diagram for Hopf bifurcation $Re_{c3}$. ■, Mode 1; □, mode 2.

from the steady symmetric flow to an oscillatory flow owing to the Hopf bifurcation at $Re = Re_{c3}$ (line with filled squares).

### 5.4. *Impinging free-shear-layer instability*

The transition diagram from the steady symmetric flow to the oscillatory flow is depicted in figure 11, which is an enlargement of figure 10. The neutral stability line for $Re_{c3}$ seems to consist of two distinct curves which intersect with each other at $A = A_{c3} \sim 2.1$. It suggests to us the existence of two different instability modes, say mode 1 and mode 2 (filled and open squares in figure 11). We expect an exchange of the two instability modes at $A = A_{c3}$. In order to confirm our expectation, we investigate the flow patterns of the disturbances. As typical examples of the two instability modes, we show two flow fields at $(A, Re) = (\frac{4}{3}, 1150)$ and $(A, Re) = (\frac{7}{3}, 850)$ in figures 12 and 13, respectively. Figure 12(*a*) is a snapshot of the time-periodic flow at the moment

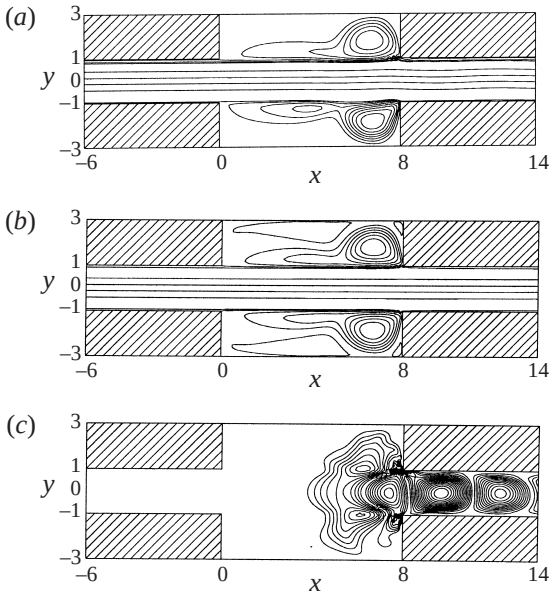


FIGURE 12. Flow patterns of mode 1. $A = \frac{4}{3}$. $Re = 1150$. (*a*) Snapshot of time-periodic flow at the moment when the velocity at $P_2(x, y) = (11.0, 0.0)$ has a maximum value. (*b*) Unstable symmetric flow. (*c*) Disturbance.

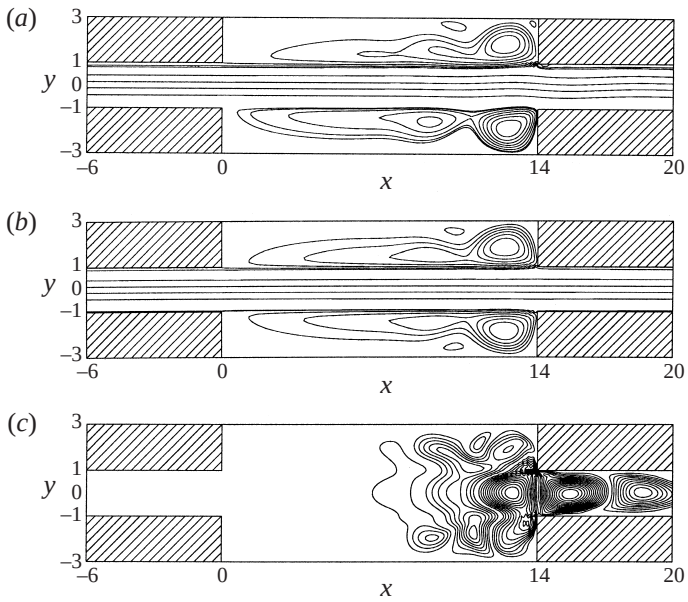


FIGURE 13. Flow patterns of mode 2. $A = \frac{7}{3}$. $Re = 850$. (*a*) Snapshot of time-periodic flow at the moment when the velocity at $P_2(x, y) = (17.0, 0.0)$ has a maximum value. (*b*) Unstable symmetric flow. (*c*) Disturbance.

when the velocity $v_2$ at $P_2(11.0, 0)$ takes a maximum value for $Re = 1150$ and $A = \frac{4}{3}$. Figure 12(*b*) shows an unstable symmetric solution at the same Reynolds number obtained by assuming the symmetry. The disturbance is calculated by subtracting the symmetric solution from the time-periodic solution as depicted in figure 12(*c*). The

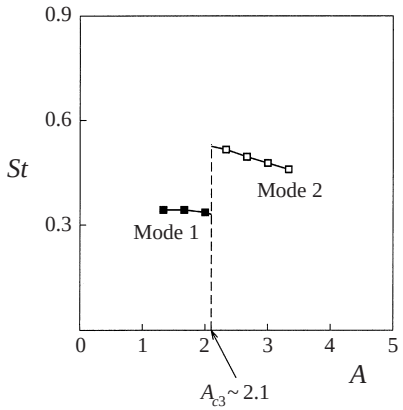


FIGURE 14. Strouhal number $St$ against the aspect ratio $A$. ■, Mode 1; □, mode 2.

disturbance at $Re = 850$ for $A = \frac{7}{3}$ is also calculated in a similar manner and flow patterns of the time-periodic flow, an unstable symmetric solution and the disturbance are depicted in figures 13($a$)–13($c$), respectively. The disturbance of flow patterns for $A = \frac{4}{3}$ has two sets of vortices, whereas the disturbance for $A = \frac{7}{3}$ consists of three sets of vortices. This difference between mode 1 and mode 2 shows the exchange of the instability modes.

We expect an abrupt change of oscillation frequency at $A = A_{c3}$ corresponding to the exchange of the instability modes. The Strouhal number $St(\equiv L_0 f / U_{max})$, where $f$ is the frequency in the time-periodic flow, is evaluated from the numerical data and is depicted in figure 14. In figure 14 the line with filled squares shows mode 1 and the line with open squares shows mode 2. The Strouhal numbers of mode 1 and mode 2 have almost a linear dependence on the aspect ratio $A$ except at $A = A_{c3}$, respectively. The Strouhal number changes stepwise at $A = A_{c3} \sim 2.1$, where the exchange of the instability modes occurs. The instability where Strouhal number changes stepwise with a continuous change of parameter is characteristic of the impinging free-shear-layer instability (IFSLI). Such an instability occurs when a jet-like stream impinges on an object which has a corner edge. This instability occurs in the channel under consideration here because the inlet flow impinges on the corners of the sudden contraction. We conclude that the mechanism of the stepwise change of $St$ in the impinging free-shear-layer instability lies in the exchange of such instability modes.

## 6. Conclusions

We have investigated transitions and instabilities of two-dimensional flow in a symmetric channel with a suddenly expanded part theoretically and experimentally as an extension of the work by Mizushima *et al.* (1996).

We obtained a more complete bifurcation diagram than MOY by calculating unstable asymmetric solutions by the finite-element method. The unstable asymmetric solutions were missing in MOY. Linear and weakly nonlinear stability theories were successfully applied to the flow and it was shown that the second pitchfork bifurcation at $Re = Re_{c2}$ changes from a supercritical to a subcritical bifurcation at $A = A_{c1} = 2.44$. The hysteresis was shown to occur in the range of $Re_{c2} \leqslant Re \leqslant Re'_{c2}$, where two stable and two unstable asymmetric solutions and a stable symmetric solution exist.

The neutral stability line for $Re_{c3}$ was shown to consist of two distinct curves which intersect each other at $A = A_{c3} \sim 2.1$. We have found an exchange of the two instability modes at $A = A_{c3} \sim 2.1$. The Strouhal number $St$ changes stepwise at $A = A_{c3} \sim 2.1$, where the exchange of the instability modes occurs. The mechanism of the stepwise change of $St$ in the impinging free-shear-layer instability (IFSLI) was revealed as a result of the exchange of the instability modes.

The authors express their cordial thanks to Professors K. Hirata and H. Yamaguchi at Doshisha University for valuable discussions. This work was partially supported by a Grant-in-Aid from the Ministry of Education, Science and Culture and also by a grant to RCAST at Doshisha University from the Ministry of Education, Japan.

## REFERENCES

Alleborn, N., Nandakumar, K., Raszillier, H. & Durst, F. 1997 Further contributions on the two-dimensional flow in a sudden expansion. *J. Fluid Mech.* **330**, 169–188.

Cherdron, W., Durst, F. & Whitelaw, J. H. 1978 Asymmetric flow and instabilities in symmetric ducts with sudden expansion. *J. Fluid Mech.* **84**, 13–31.

Durst, F., Melling, A. & Whitelaw, J. H. 1974 Low Reynolds number flow over a plane symmetric sudden expansion. *J. Fluid Mech.* **64**, 111–128.

Fearn, R. M., Mullin, T. & Cliffe, K. A. 1990 Nonlinear flow phenomena in a symmetric sudden expansion. *J. Fluid Mech.* **211**, 595–608.

Mizushima, J. & Shiotani, Y. 2000 Structural instability of the bifurcation diagram for two-dimensional flow in a channel with a sudden expansion. *J. Fluid Mech.* **420**, 131–145.

Mizushima, J., Okamoto, H. & Yamaguchi, H. 1996 Stability of flow in a channel with a suddenly expanded part. *Phys. Fluids* **8**, 2933–2942.

Rockwell, D. & Naudascher, E. 1979 Self-sustained oscillations of impinging free shear layers. *Ann. Rev. Fluid Mech.* **330**, 67–94.